Kinetic, Spectroscopic, and Structural Investigations of the Soybean Lipoxygenase-1 First-Coordination Sphere Mutant, Asn694Gly † , ‡

9 AUTHORS, INCLUDING:

Maksymilian Chruszcz
University of South Carolina
140 PUBLICATIONS **2,526** CITATIONS

SEE PROFILE

Wladek Minor
University of Virginia
204 PUBLICATIONS **37,736** CITATIONS

SEE PROFILE

Kinetic, Spectroscopic, and Structural Investigations of the Soybean Lipoxygenase-1 First-Coordination Sphere Mutant, Asn694Gly[†,‡]

Erika N. Segraves,[§] Maksymilian Chruszcz,[||] Michael L. Neidig,[⊥] Viola Ruddat,[§] Jing Zhou,[⊥] Aaron T. Wecksler,[§] Wladek Minor,[||] Edward I. Solomon,*,[⊥] and Theodore R. Holman*,[§]

Department of Chemistry and Biochemistry, University of California, Santa Cruz, California 95064, Department of Molecular Physiology and Biological Physics, University of Virginia, Charlottesville, Virginia 22908, and Department of Chemistry, Stanford University, Stanford, California 94305

ABSTRACT: In wild-type soybean LO-1 (WT sLO-1), Asn694 is a weak sixth ligand that is thought to be critical for enzymatic catalysis. In this investigation, N694G sLO-1 was studied to probe its contribution at this sixth ligand position to the kinetic and spectroscopic properties. The k_{cat} value of N694G is ∼230 times lower than that of WT sLO-1 at 25 °C, which can be partially explained by a lowered reduction potential of the iron as seen as a shift in the visible ligand-to-metal charge-transfer band ($\lambda_{max} = 410$ nm for N694G and $\lambda_{max} = 425$ nm for WT sLO-1). This conclusion was supported by a faster rate of oxidation of N694G by the product than that of WT sLO-1 ($k_2 = 606$ s^{-1} for N694G and $k_2 = 349$ s^{-1} for WT sLO-1). These results suggest a stronger ligand at the active site iron than the native Asn694, which is confirmed to be a water bound to the Fe(II) in the crystal structure. This produces a six-coordinate circular dichroism/magnetic circular dichroism (CD/MCD) spectra for ferrous N694G and an intermediate rhombic electron paramagnetic resonance (EPR) signal for ferric N694G. The EPR spectrum and its pH dependence suggest that the coordination environment of ferric N694G contains one hydroxide and one water. On the basis of both kinetic and structural factors, we propose that the Asn694 water-derived ligand would likely be a hydroxide and the active site, water-derived ligand a water in the ferric state, hence lowering the reaction rate of N694G more than would be expected from the lowered reduction potential alone.

Lipoxygenase (LO) is a mononuclear, non-heme iron dioxygenase that catalyzes the incorporation of molecular oxygen into a 1,4-*cis*,*cis*-pentadiene fatty acid to form hydroperoxide products. In plants, soybean LO isoform-1 (sLO-1)[1] oxygenates linoleic acid (LA) with positional specificity to produce 13(*S*)-hydroperoxy-9(*Z*),11(*E*)-octadecadienoic acid [13-(*S*)-HPOD], which is a precursor to potent signaling molecules in growth regulation (*1*) and wound response (*2*). In humans, the lipoxygenase products are members of the eicosanoid family and are implicated in asthma (*3*), heart disease (*4*), and various cancers (*5*).

LO catalyzes the addition of molecular oxygen by substrate activation rather than O$_2$ activation (*6*). In the generally accepted mechanism (Scheme 1), the inactive, ferrous enzyme (resting LO) reacts with 13-(*S*)-HPOD to generate the catalytically active ferric enzyme [called yellow LO due to a ligand-to-metal charge-transfer (LMCT) band ($\lambda_{max} \sim$ 425 nm)] (*7*, *8*). The catalytic cycle then begins with the

Fe(III)−OH$^-$ species abstracting the *pro-S* hydrogen atom from the 1,4-*cis*,*cis*-pentadiene fatty acid substrate to form a pentadienyl radical and the Fe(II)−OH$_2$ intermediate (Scheme 1) (*9*, *10*). A large, temperature-independent kinetic isotope effect (KIE) has been reported for sLO-1 to be ∼80 (*11*) and for human 15-LO (15-hLO) to be ∼50 (*12*, *13*), indicating that cleavage of the C−H bond is the rate-determining step. The substrate radical reacts with O$_2$, delivered via an oxygen channel (*14*, *15*), generating a peroxyl radical, which is reduced as a result of a hydrogen atom transfer from the Fe(II)−OH$_2$ species, to produce the hydroperoxide product and the Fe(III)−OH$^-$ form of the enzyme. Finally, the purple LO species, named for the

* To whom correspondence should be addressed. T.R.H.: phone, (831) 459-5884; fax, (831) 459-2935; e-mail, tholman@chemistry.ucsc.edu. E.I.S.: phone, (650) 723-4694; fax, (650) 725-0259; e-mail, edward.solomon@stanford.edu.

[§] University of California.

[||] University of Virginia.

[⊥] Stanford University.

[1] Abbreviations: hLO, human lipoxygenase; WT sLO-1, wild-type soybean lipoxygenase-1; sLO-3, soybean lipoxygenase-3; purple lipoxygenase, 13-(*S*)-HPOD-bound Fe(III) enzyme; Fe(II)·HPOD, complex of Fe(II) and 13-(*S*)-HPOD; N694G, mutation of Asn694 to glycine; LA, linoleic acid; AA, arachidonic acid; 13-(*S*)-HPOD, 13-(*S*)-hydroperoxy-9(*Z*),11(*E*)-octadecadienoic acid (the principle oxidation product of LA); 13-(*S*)-HODE, 13(*S*)-hydroxy-9(*Z*),11(*E*)-octadecadienoic acid (the reduced oxidation product of LA); 9-(*S*)-HPOD, 9(*S*)-hydroxy-9(*E*),11(*Z*)-octadecadienoic acid; 9-(*S*)-HODE, 9(*S*)-hydroperoxy-9(*Z*),11(*E*)-octadecadienoic acid; LA-D31, fully deuterated LA; 15-(*S*)-HPETE, 15(*S*)-hydroperoxyeicosatetraeonic acid (the oxidation product of AA); CD, circular dichroism; MCD, magnetic circular dichroism; LMCT, ligand-to-metal charge transfer; K_D, dissociation constant of the enzyme−P complex; k_2, rate constant of peroxide scission; k_{obsd}, observed pseudo-first-order rate constant; k_{cat}, rate constant for product release; k_{cat}/K_m, rate constant for substrate capture; KIE, primary kinetic isotope effect; k^H_{cat}/k^D_{cat}, KIE for k_{cat}; $(k^H_{cat}/K_m)/(k^D_{cat}/K_m)$, KIE for k_{cat}/K_m.

Scheme 1:   Lipoxygenase Mechanism
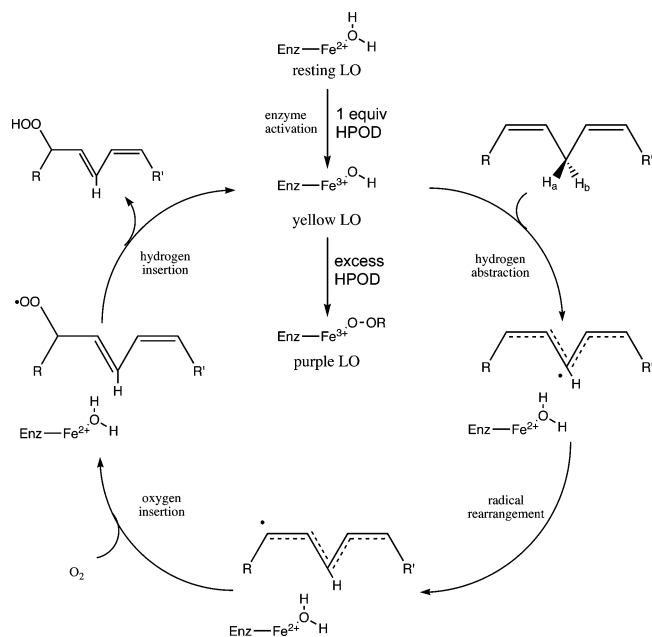
peroxide-to-Fe(III) charge-transfer band ($\lambda_{max} = 580$ nm), can be formed by addition of excess 13-(*S*)-HPOD to yellow LO; however, it is unclear if this species is generated during catalysis.

The crystal structures of two soybean lipoxygenases, sLO-1 (*16*) and sLO-3 (*17*), and one rabbit 15-lipoxygenase (*18*) (15-rLO) have been reported. Five residues that serve as ligands for the iron-binding site have been shown to be highly conserved across plant and mammalian lipoxygenases; however, a key difference arises in the sixth amino acid ligand of the active site. In most plant lipoxygenases, mammalian 5-LOs, and murine/human platelet 12-LOs, the sixth ligand is Asn (*19*). In the remaining 12-LOs and reticulocyte 15-LOs, however, the ligand is His (*19*). Additionally, sequence comparison shows the ligand to be a Ser in 15-hLO-2 (*20, 21*) and in mouse 8-LO (*22*). This difference in coordination has continued to be of interest in our labs because of its relationship with enzyme activity.

WT sLO-1, with an Asn ligation, is the best characterized lipoxygenase, both kinetically and spectroscopically. Utilizing MCD, it was determined that Asn694 was highly flexible and the Fe(II)−Asn bond could vary in length depending on the experimental conditions (*23*). In particular, the ferrous form of the enzyme exists as a 60:40 mixture of five- and six-coordinate species, with the Asn varying between bound and unbound. However, when a substrate (linoleic acid) or an inhibitor (oleic acid) was added, the coordination environment changed to 100% six-coordinate, suggesting a structural connection between the active site and the Asn694 ligand (*23, 24*). This hypothesis of a structural connection between the active site and the iron coordination environment was confirmed by mutating a hydrogen bond network (Gln495, Gln697, and Asn694), which affected the ability of substrate binding to change the iron coordination and subsequently enzyme activity (*25, 26*).

The importance of Asn694 in sLO-1 was also confirmed when the Asn was mutated to His (N694H). The ferrous MCD of N694H manifested only a six-coordinate species, not a mixture of five- and six-coordinate species, due to the

strong ligation of the histidine (*24*). In addition, the ligation of the His reduced the reactivity of sLO-1, due to a decrease in its reduction potential and hence a lowered rate of hydrogen abstraction. It should be noted that this His ligation is found naturally in 15-hLO, whose decreased activity relative to that of 15-sLO was previously proposed to be due to its lowered reduction potential (*27*).

In our study, we further examine the role of Asn694 in sLO-1 by performing kinetic, spectroscopic, and structural investigations of point mutant Asn694Gly sLO-1 (N694G), which possesses a coordination environment different from that of WT sLO-1 and manifests a dramatically lowered enzymatic activity.

MATERIALS AND METHODS

Materials. LA was purchased from Aldrich Chemical Co., and perdeuterated linoleic acid (LA-D31) was purified from a mixture of perdeuterated algal fatty acids from Cambridge Isotope Labs, as previously described (*24*). All commercial fatty acids were repurified using a Higgins SemiPrep Haisil (25 cm × 10 mm) C-18 column. Solution A was 99.9% MeOH and 0.1% acetic acid, while solution B was 99.9% H_2O and 0.1% acetic acid. An isocratic elution of 85% A and 15% B was used to purify all fatty acids, and they were stored at −80 °C for a maximum of 6 months. All other chemicals were reagent grade or better and were used without further purification.

Mutagenesis, Overexpression, and Purification of Lipoxygeanse. Site-directed mutagenesis, overexpression, and purification of WT and N694G followed a protocol outlined previously (*24*). In brief, following expression of the protein in BL21-DE3 (*Escherichia coli*), the cells were harvested by centrifugation and their membranes were disrupted by sonication. Cell debris was pelleted, and the supernatant was first dialyzed against 20 mM Bis-Tris buffer (pH 6.0) and then applied to a SP-Sephadex high-flow ion exchange column (Pharmacia), which was equilibrated with the same buffer. Eluted fractions containing lipoxygenase activity were pooled, concentrated, dialyzed against 20 mM Bis-Tris buffer (pH 6.0), and applied to a Macro-Prep 25-S ion exchange column (Bio-Rad). After concentration and buffer exchange into 0.1 M borate (pH 9.2), the isolated enzyme was estimated to be greater than 90% pure (SDS−PAGE). The iron contents of all lipoxygenase enzymes were determined on a Finnegan inductively coupled plasma mass spectrometer (ICP-MS) using internal standards of Co(II)−EDTA, and data were compared with standardized iron solutions.

Enzyme Activation Kinetics. Activation kinetics were assessed as previously described (*8, 28*). Briefly, kinetic measurements of the enzyme activation were performed under pseudo-first-order conditions (with the enzyme as the minor component) using a DX·17MV Applied Photophysics spectrofluorometer equipped with a 150 W xenon arc lamp light source and a 320 nm cutoff filter. The oxidation of ferrous N694G and WT sLO-1 was observed as a temporal change in the fluorescence emission above 320 nm ($\lambda_{ex} = 280$ nm). The assay samples were ∼2 μM enzyme (WT or N694G) over a range of 40 μM to 2.5 mM 13-(*S*)-HPOD in a mixed buffer (25 mM Tris, 25 mM Ches, and 25 mM Caps buffers, 50 mM ionic strength, pH 9.2, and 25 °C). To determine K_D and k_2 values, kinetic runs were performed at

seven different concentrations of 13-(S)-HPOD; each peusdo-first-order rate constant (k_{obsd}) was the average of five determinations. The stopped-flow apparatus was rinsed with HNO_3, KOH, and water periodically to prevent kinetic artifacts from enzyme buildup.

Steady-State Kinetic Measurements. Steady-state kinetic values were determined by following the formation of the conjugated product at 234 nm ($\epsilon = 2.5 \times 10^4$ M^{-1} cm^{-1}) with a Perkin-Elmer Lambda 40 spectrophotometer. No photodegradation of the product was observed. All kinetic measurements were standardized to iron content. The assay samples were 2 mL in volume with substrate concentrations ranging from 1 to 100 μM and were constantly stirred with a rotating magnetic bar. A stock solution of LA was prepared in 95% ethanol and diluted into buffer so that the total ethanol concentration was less than 1.5%. Fatty acid concentrations were verified by allowing the enzyme reaction to proceed to completion and quantitating the conjugated product at 234 nm. Higher substrate concentrations were avoided due to the formation of micelles, which would alter the free substrate concentration (29). Initial rates (up to the first 15% of the reaction) for each substrate were fitted to the Michaelis−Menten equation using KaleidaGraph (Synergy) and errors determined. All subsequent kinetic measurements were handled in a similar fashion. Kinetic measurements were determined at pH 9.2 in a mixed buffer (25 mM Tris, 25 mM Ches, and 25 mM Caps buffers) at 25 °C. The total ionic strength was adjusted to 50 mM via the addition of NaCl. The temperature was controlled using a circulating water bath and jacketed cuvette system.

Kinetic Isotope Effect. The KIE values were determined by comparing steady-state results using pure protio and pure perdeuterated LA substrate and should be differentiated from competitive KIE values where there is a mixture of proteo and deutero substrate in the same reaction flask. Steady-state KIE values were determined by following the formation of the conjugated product at 234 nm, as discussed above, and these experiments were carried out in 0.1 M borate buffer (pH 9.2) with the temperature-controlled circulating water bath and jacketed cuvette system. For protonated LA, ≈120 nM N694G was used, and for the D-LA, ≈340 nM N694G was used for each assay (normalized to iron content).

Reaction Rates at Varying O_2 Concentrations. Reaction rates of N694G were determined by measuring oxygen consumption on a Clark oxygen monitor as previously described (30). Reactions were carried out as a function of oxygen concentration in 1 mL solutions, which were constantly stirred and thermostated to 20 °C. The reaction was initiated by the addition of ≈50 nM N696G (normalized to iron content) via a gastight Hamilton syringe to the reaction chamber. The experiments were repeated at a number of different concentrations of oxygen, established by passing mixtures of N_2 and O_2 over stirred solutions in the reaction chamber for 20 min. The new oxygen concentration was calibrated against the value of O_2 dissolved in an air-saturated solution at 20 °C (288 μM O_2). The rate of oxygen consumption was recorded at O_2 concentrations from 5 to 300 μM.

Enzymatic Product Analysis. Oxidation products were produced by reaction of LA with sLO-1 and N694G. The reactions were quenched with glacial acetic acid to pH 3, and the mixtures were exhaustively extracted with ethyl acetate, reduced to the alcohol with trimethyl phosphite, and evaporated to dryness (12). The samples were then reconstituted into methanol and injected into a Thermo Finnegan LTQ-ESI apparatus, and the parent peak at m/z 295 fragmented with a collision energy of 35 eV. These spectra were subsequently compared to standard curves of 13(S)-hydroxy-9(Z),11(E)-octadecadienoic acid [13-(S)-HODE] and 9(S)-hydroxy-9(E),11(Z)-octadecadienoic acid [9-(S)-HODE] (purchased from BIOMOL) and their relative percentages determined by comparing the unique peak for 13-(S)-HODE at m/z 179 against the unique peak for 9-(S)-HODE at m/z 171.

UV−Vis Absorption and CD Spectroscopies. The UV−vis absorption spectra were recorded on a Perkin-Elmer Lambda 40 monochronometer. Spectra were recorded in 0.1 M borate (pH 9.2) at an ionic strength of 0.1 M (adjusted with NaCl) at 4 °C. CD absorption spectra were obtained using an Aviv 60DS spectropolarimeter in 0.1 M borate (pH 9.2). CD spectra were baseline corrected by subtracting the buffer and cell background from the raw data. Titrations were performed by the addition of 1 equiv of 13-(S)-HPOD to 0.6 mL of lipoxygenase (20 mg/mL).

CD and MCD Spectroscopy. Near-infrared (600−2000 nm) CD and MCD data were recorded on a Jasco J-200D spectropolarimeter with a liquid N_2-cooled InSb detector and equipped with an Oxford Instruments SM4000 7 T superconducting magnet/cryostat capable of fields of ≤7 T and temperatures of ≥1.5 K. The N694G CD sample (∼1.8 mM) was exchanged into deuterated CHES buffer (50 mM, pD 9.2) and kept at 5 °C during data collection with a circulating cooling bath attached to the sample holder. Glycerol-d_3 was added at 60% (v/v) to the N694G/Fe(II) solution for preparation of the MCD sample, and CD spectra were recorded with and without glycerol addition to ensure that the site was unaffected by the glassing agent (note that no change in the CD spectrum due to glycerol was observed). CD spectra were corrected for buffer and cell baselines by subtraction. Low-temperature MCD data were obtained in custom-made cells consisting of two Infrasil quartz disks separated by a 0.3 cm thick neoprene O-ring spacer into which the sample was injected and secured between two copper plates. The MCD spectrum was corrected for the natural CD and zero-field baseline effects caused by strain in the glasses by averaging the positive and negative field data at a given temperature [i.e., (7 T−7 T)/2].

EPR Spectroscopy. EPR measurements were performed on a Bruker ESP-500E spectrometer equipped with a dual-mode X-band cavity and an Oxford Instruments ESR-900 helium flow cryostat. HAM (M. Hendrich, Carnegie Mellon University, Pittsburgh, PA) was used for data manipulation and EPR spectral simulation, as described previously (24). In brief, the signals were fit with an effective $S = {}^1/_2$ model which uses a g-dependent line width and properly accounts for field-dependent transition probabilities. The temperature dependence was also fit with this program using the standard Boltzmann equation. The amount of EPR-active Fe(III) in the protein samples was determined relative to an Fe(III)−EDTA standard. A 100 μM Fe solution was made from a 1000 ppm iron standard (Fischer Scientific), with addition of a 10-fold excess of EDTA in 25% glycerol. The EPR spectra were recorded at a modulation frequency of 100 kHz and at microwave frequencies of ∼9.63 GHz. Precise

Table 1: Data Collection and Refinement Statistics for N694G[a]

data collection	
wavelength (Å)	1.0311
resolution range (Å)	50.00−1.95
no. of unique reflections	60260
R_{merge}	0.044 (0.333)
completeness (%)	95.9 (91.0)
average redundancy	2.8 (2.7)
average $I/\sigma(I)$	21.3 (3.1)
refinement	
resolution (Å)	33.00−1.95
no. of unique reflections	56381
completeness (%)	96.1 (91.0)
R (%)	18.0 (20.5)
R_{free} (%)	23.2 (28.3)
no. of non-H atoms	7191
no. of water molecules	676
rmsd for bond lengths (Å)	0.019
rmsd for bond angles (deg)	1.68
rmsd for torsion angles (deg)	6.49
average B factor (Å^2)	28.84
Ramachandran plot	
residues in the most favored region (%)	90.7
residues in additional allowed regions (%)	9.2
residues in disallowed regions (%)	0.1

[a] The data for the highest-resolution shell (2.02−1.95 Å) are reported in parentheses.

Table 2: Comparison of Kinetic Parameters for WT, N694G, and N694H sLO-1[a]

	k_{cat}[b] (s^{-1})	k_{cat}/K_M[b] (μM^{-1} s^{-1})	$k_{cat(O_2)}$[c] (s^{-1})	$k_{cat}/K_{M(O_2)}$[c] (μM^{-1} s^{-1})
WT	266 (22)	18 (5)	230 (15)[d]	7.5 (0.9)[d]
N694G	1.17 (0.02)	0.4 (0.2)	0.71 (0.01)	≥0.7[e]
N694H (24)	10 (2)	2.5 (1.1)	nd[f]	nd[f]

[a] Numbers in parentheses represent errors as determined from replicate determinations. [b] Data were collected at 25 °C. [c] Data were collected at 20 °C. [d] From ref 15. [e] $K_{M(O_2)}$ too low to be measured (≤1 μM). [f] Not determined.

microwave frequencies were recorded for individual spectra to ensure precise *g*-alignment. Other EPR parameters are specified in the figure legends.

Crystallization and Data Collection. Crystals of N694G were grown and cryoprotected as previously described (16, 25). The 100 K data were collected at the Structural Biology Center beamline 19BM at Argonne National Laboratory (Argonne, IL) and processed with HKL2000 (31). The N694G crystal was monoclinic in the $P2_1$ space group with the following unit cell parameters: a = 92.88 Å, b = 92.84 Å, and β = 90.7°. The structure of native soybean lipoxygenase-1 (PDB entry 1F8N) was used as an initial model.

Crystallographic Refinement. Refinement of the mutant structures was performed with REFMAC (32), O (33), and COOT (34). For R_{free} calculations, a subset of 5.1% reflections was used (35). During the refinement, the occupancies of the ferrous ion and its coordinating water molecules were adjusted to 0.7 as for previous LO mutants (25). This resulted in an average displacement factor of the iron-coordinating atoms (27 Å^2), which is similar to the value of the Fe(II) displacement parameter (29 Å^2) and closer to the average B factor for all atoms of the structure (Table 1). PROCHECK (36) and MOLPROBITY (37) were used for structure validation. Residues Val312, Asn534, and Ser560 have unusual backbone conformations, as observed for other LO mutants (25). The coordinates and structure factors were deposited in the Protein Data Bank as entry 1Y4K. Superpositions of molecules or their fragments were carried out using LSQKAB (38) from the CCP4 package (39). Figures were prepared with PyMOL (40).

RESULTS AND ANALYSIS

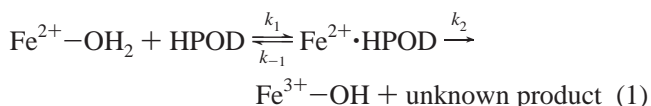*Protein Purification and Kinetic Determinations*

N694G and WT sLO-1 were purified with yields of 2−4 mg/L, with metal contents of 50 ± 10 and 80 ± 5%, respectively. The activation of N694G and WT sLO-1 can

be described by eq 1:

$$Fe^{2+}-OH_2 + HPOD \underset{k_{-1}}{\overset{k_1}{\rightleftharpoons}} Fe^{2+} \cdot HPOD \overset{k_2}{\rightarrow}$$
$$Fe^{3+}-OH + unknown\ product\ (1)$$

where the term K_D will be used as previously defined: $K_D = K_M$, since $(k_{-1} + k_2)/k_1 = K_M$ and $k_{-1} \gg k_2$ (41, 42). N694G and WT sLO-1 exhibited saturation curves consistent with formation of the oxidized ferric enzyme [yellow LO, Fe(III)−OH$^-$]. Using nonlinear regression methods, the dissociation constant (K_D) and the rate constant (k_2) were determined for N694G and WT sLO-1. 13-(S)-HPOD binds to N694G with a K_D of 41 ± 5 μM, which was comparable to that of WT sLO-1 (39 ± 14 μM). The rate of oxidation of the iron center for N694G was twice that of WT sLO-1 (k_2 = 606 ± 18 and 349 ± 31 s^{-1}, respectively). The K_D and k_2 values for WT sLO-1 differ slightly from our previously reported values, presumably due to differences in buffer composition (8).

The steady-state parameters, k_{cat} and k_{cat}/K_M (Table 2), were determined at 25 °C; the k_{cat} value of N694G was ∼230 times lower than that of WT sLO-1, while the k_{cat}/K_M value was ∼45 times lower. The KIE data indicate similar mechanistic rate-limiting steps for N694G and WT sLO-1. The $^Dk_{cat}$ of N694G exhibited temperature independence (average $^Dk_{cat}$ = 37 ± 3), over the range of 15−37 °C (Supporting Information). Although the magnitude of the KIE is lower than that observed for previous mutants (24, 25), the magnitude of the $^Dk_{cat}$ is much larger than semiclassical theory predicts (KIE = 7−10) and is consistent with a tunneling mechanism for hydrogen atom abstraction (43). A large, temperature-independent $^Dk_{cat}$ is also seen for WT sLO-1, indicating hydrogen atom abstraction is fully rate limiting (44). The analysis of $^Dk_{cat}/K_M$ was hampered by high errors due to extrapolation from the steady-state K_M values; however, the overall trend indicates a slight temperature dependence, with a maximum of 44 ± 19 at 37 °C. The data for N694G are comparable to our previous data for N694H, which manifested a large $^Dk_{cat}/K_M$ of 60 ± 9 at 30 °C (24).

The kinetic parameters at varying O$_2$ concentrations were analyzed at saturating LA concentrations (5K_M) at 20 °C (Table 2). The $k_{cat(O_2)}$ was determined to be 0.71 ± 0.01 s^{-1} for N694G, which is in good agreement with the k_{cat} values determined spectrophotometrically (Table 2) and ∼320-fold lower than the $k_{cat(O_2)}$ for WT sLO-1 (230 ± 15 s^{-1}) (15). There was no decrease in the rate between 5 and 260 μM O$_2$, which indicates that the $K_{M(O_2)}$ is less than 1 μM O$_2$ and therefore the $k_{cat}/K_{M(O_2)}$ value is ≥0.7 μM^{-1} s^{-1}. For WT
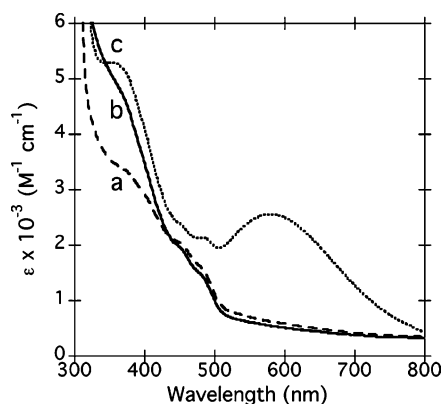
FIGURE 1: UV−vis absorbance spectra of (a) ferrous N694G (− − −), (b) yellow N694G (−), and (c) purple N694G (•••) at 4 °C. Samples were corrected for iron content.
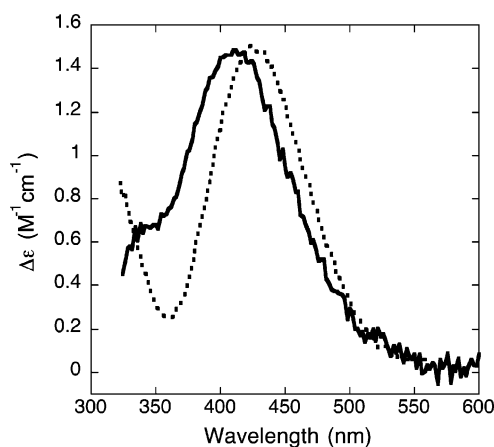

FIGURE 2: CD spectra of yellow WT sLO-1 (•••) and yellow N694G (−) at 4 °C. Samples were corrected for iron content.
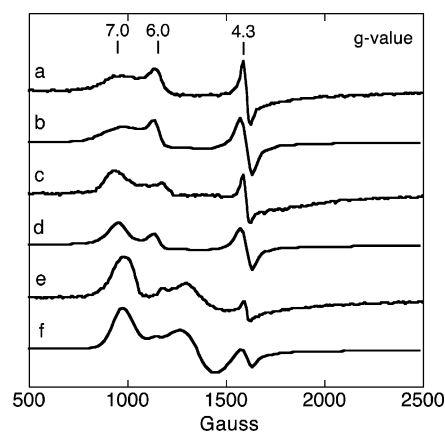

FIGURE 3: EPR spectra of N694G: (a) yellow form, 0.1 M borate, pH 9.2; (b) simulation with 64 ± 6% intermediate rhombicity, 28 ± 3% axial, and 8 ± 2% rhombic; (c) yellow form, 0.1 M Tris, pH 7.2; (d) simulation with 76 ± 7% intermediate rhombicity, 18 ± 2% axial, and 6 ± 2% rhombic; (e) purple form, 0.1 M borate, pH 9.2; and (f) simulation with 96 ± 2% intermediate rhombicity, 2 ± 1% axial, and 2 ± 1% rhombic. Experimental parameters for all spectra: concentration, 150 μM Fe(III); ionic strength, 0.1 M; temperature, 4 K; field set, 4000 G; scan range, 8 kG; time constant, 82 ms; modulation amplitude, 8 G; microwave power, 200 μW; frequency, 9.63 GHz; and gain, 60.

sLO-1, the $k_{cat}/K_{M(O_2)} = 7.5 \pm 0.9$ μM^{-1} s^{-1} [$K_{M(O_2)} = 30 \pm 4$ μM^{-1} s^{-1}] (15), which is 11-fold higher than that for N694G; however, due to the limitations of the $K_{M(O_2)}$ experiment, these values could be closer.

WT sLO-1 is known to oxidize LA with high regio resolution. Accordingly, the chemically reduced, hydroperoxide products of both WT sLO-1 and N694G were analyzed by MS/MS, and the ratio of 13-HPOD to 9-HPOD was approximately 97:3, consistent with published results (45). This result indicates that the bound substrate is similar to that of WT sLO-1 and is not inverted as seen at low pH, which increases the 9-HPOD concentration relative to that of 13-HPOD (45).

Spectroscopy and Crystallography

Fe(III) Site. Oxidation of N694G was accompanied by an increase at approximately 400 nm (Figure 1b), due to the LMCT band, characteristic of the yellow species [Fe(III)−OH$^-$] (24). UV−vis CD spectroscopy resolved the LMCT feature from the large protein envelope and revealed a distinct, well-resolved band, with a maximum at 410 nm (Figure 2). This LMCT band is higher in energy than WT sLO-1 (425 nm), which is consistent with a decrease in reduction potential of the iron, relative to WT sLO (24). The Δε value was corrected for iron content and is comparable in magnitude to that of WT sLO-1 (Δε = 1.50 M^{-1} cm^{-1} for N694G and Δε = 1.45 M^{-1} cm^{-1} for WT sLO-1).

Addition of excess 13-(S)-HPOD to N694G produced the purple species [Fe(III)−13-(S)-HPOD], which is due to a peroxide-to-Fe(III) LMCT (Figure 1c) (46). N694G exhibited a maximum at 590 nm (ε = 1750 M^{-1} cm^{-1}), while WT sLO-1 exhibited a maximum at 595 nm (ε = 1510 M^{-1} cm^{-1}) (24). Previously, our labs reported a maximum at 580 nm (ε = 1550 M^{-1} cm^{-1}) for WT sLO-1 under different buffer conditions (28), indicating a buffer dependence of this LMCT.

The EPR spectrum of as-isolated N694G (150 μM iron) in a frozen solution at 4 K exhibited a weak g ∼ 4.3 signal (data not shown). The low intensity of this signal represents less than 1% of the total iron and indicates that the enzyme is mostly in its ferrous state. Addition of 1 equiv of 13-(S)-HPOD to ferrous N694G oxidized the iron to the catalytically competent yellow, ferric species. Yellow N694G at pH 9.2 (0.1 M borate and ionic strength of 0.1 M) exhibited a complex multicomponent EPR signal with pronounced g ≈ 4.3, 6, and 7 features (Figure 3a). In the analysis of the EPR spectrum of yellow N694G (pH 9.2), the g ≈ 6 signal had axial symmetry (E/D = 0), the g = 7 signal had intermediate rhombicity (E/D = 0.05), and the g = 4.3 signal had rhombic symmetry (E/D = 0.33). These features indicate that the yellow N694G form at pH 9.2 contained no less than three species: axial (E/D = 0, g_x, g_y, and g_z = 6, 6, and 2, respectively), intermediate rhombicity (E/D = 0.05, g_x, g_y, and g_z = 7.0, 4.0, and 1.9, respectively), and rhombic (E/D = 0.33, g_x, g_y, and g_z = 4.3, 4.3, and 4.3, respectively). Addition of an additional 3 equiv of 13-(S)-HPOD generated the purple species at pH 9.2 (0.1 M borate and ionic strength of 0.1 M) with a different EPR spectrum with three, major g ≈ 4.3, 5.0, and 7.0 features (Figure 3e). The multicomponent spectrum of purple N694G (pH 9.2) was comprised of the same three species as the yellow enzyme form, one major signal (E/D = 0.05, g_x, g_y, and g_z = 7.0, 5.0, and 1.9, respectively) and two minor signals with E/D values of 0.33 and 0, respectively, but in different ratios. The yellow and

Table 3: Theoretical EPR Simulation Parameters

	E/D	g_x $(\Delta g)^a$	g_y $(\Delta g)^a$	g_z $(\Delta g)^a$
Sim axial	0.0	6.0 (0.1)	6.0 (0.8)	2.0 (0.1)
Sim intermediate rhombic 1 (yellow, pH 9.2)	0.05	7.0 (0.6)	5.0 (0.8)	1.9 (0.8)
Sim intermediate rhombic 2 (yellow, pH 7.2)	0.05	7.0 (0.3)	5.0 (1.0)	1.9 (1.0)
Sim intermediate rhombic 3 (purple, pH 9.2 and 7.2)	0.05	7.0 (0.4)	5.0 (0.4)	1.9 (0.4)
Sim rhombic 1	0.33	4.3 (0.1)	4.3 (0.1)	4.3 (0.1)
Sim rhombic 2	0.33	4.5 (0.1)	4.3 (0.1)	4.0 (0.1)

^{a} Line widths in g-values at half-height of the absorption curve are given in parentheses.

Table 4: Iron−Ligand Bond Distances of WT sLO-1 and N694G, in Angstroms^a

	WT (1F8N)	N694G (1Y4K)
His499 Nϵ2	2.21, 2.24	2.35
His504 Nϵ2	2.34	2.19
His690 Nϵ2	2.29	2.31
Asn694 Oδ1	2.87	2.14 (OH$_2$ 1003)
Ile839 O1	2.28	2.20
OH$_2$ 841	2.11	2.27 (OH$_2$ 1002)

^{a} Equivalent residues noted in parentheses.

purple species were also generated at pH 7, to determine any pH dependence. The EPR spectrum of yellow N694G at pH 7.2 (0.1 M Tris and ionic strength of 0.1 M) contained the same three species as at pH 9.2, except the relative amount of the axial species at $g = 6$ is decreased (Figure 3c). The spectrum of purple N694G at pH 7.2 was identical to the spectrum at pH 9.2 (data not shown). For all spectra, features with g values around 2 were obscured by an adventitious Cu(II) signal.

The quantification of the amount of Fe(III) contributing to the axial ($g \approx 6$), intermediate rhombicity ($g \approx 7.0$), and rhombic ($g \approx 4.3$) signals, for all the samples measured, was complicated by the fact that the axial and intermediate rhombicity signals spread over a large field range (≈ 2300 G) and overlap. This problem was overcome by EPR spectral simulations. The simulated spectra were simultaneously integrated over the entire field range to obtain the total EPR intensity from transitions within the $M_s = \pm^1/_2$ Kramers doublet for the axial and intermediate rhombicity signals and the middle transition of the rhombic signal. The Fe(III)−EDTA standard was used for spin quantitation. The double integral was evaluated between 0 and 2500 G, just short of the interfering signal from adventitious Cu(II). The signals for both the yellow and purple species of N694G were simulated with an effective spin $S' = ^1/_2$ Hamiltonian (Figure 3b,d,f), with the parameters given in Table 3. An axial doublet ($g \approx 6$), a doublet with intermediate rhombicity ($g \approx 7.0$), and two rhombic doublets ($g \approx 4.3$) were required for the simulation. The axial simulation parameters were used previously for WT sLO, while the intermediate simulations are distinct from that published for N694H (*24*). It should be noted that for all of the intermediate rhombicity signal simulations of both the yellow and purple species, it was difficult to match the variability of the g strain of each g component. Therefore, these simulations are approximations to the true signal shape. Two rhombic doublets were required because one would not adequately fit the broad base of the $g \approx 4.3$ signal. These two rhombic components are considered as a single species in the following discussion. The simulation areas were adjusted for the g_{ave} differences of the rhombic and axial signals as described by Aasa and Vangård (*47*), and line width broadening was applied to each g value.

Quantification of the signal intensity was dependent on the relative populations of the spin manifolds of each of the three EPR active species. To account for the spin populations of all the three M_s doublets, the ZFS parameters were approximated for each species from the temperature dependence of the EPR spectral intensity over the range of 3.8−

40 K under nonsaturating conditions. The temperature dependence of the $g \approx 7.0$ and $g \approx 4.3$ signals was evaluated, and their signal intensity versus temperature was compared to the previous data for N694H. On the basis of this comparison, the ZFS of the $g \approx 7.0$ signal for both the yellow and purple species was determined to have a positive D value of approximately 2 cm^{-1}, while the rhombic $g \approx 4.3$ signal (present in the spectra of both the yellow and purple species) had a $|D|$ of approximately 1 cm^{-1}. These approximate ZFS parameters were used to calculate the Boltzmann population distributions of the three doublets, and the spin populations were corrected accordingly for the two signals [$g \approx 7$ (for both the yellow and purple species) and $g \approx 4.3$]. The observed $g \approx 6$ signal had significant spectral overlap with the other two species, and therefore, its temperature dependence could not be obtained accurately from the EPR spectral data. Its D value was set to 2 cm^{-1}, based on the fact that in WT sLO-1 two axial signals are observed with D values of approximately 2 cm^{-1} (*48*).

Utilizing the intensity simulation (g_{ave} corrected), we determined that the relative concentrations of the three EPR visible species for yellow N694G (pH 9.2) were $28 \pm 3\%$ for the axial, $64 \pm 6\%$ for the intermediate rhombicity, and $8 \pm 2\%$ for the rhombic (Figure 3b). For the yellow species at pH 7.2, the three species remained, but their relative concentrations changed to $18 \pm 2\%$ for the axial, $76 \pm 8\%$ for the intermediate rhombicity, and $6 \pm 2\%$ for the rhombic species (Figure 3d). It is important to note the dominant signal present in yellow N694G at both pH 9.2 and 7.2 was the intermediate rhombicity species ($E/D = 0.05$) at $g_{eff} = 7$, although it does not appear in the spectrum to be the largest feature. The dominant signal in purple N694G (pH 9.2) is also the intermediate rhombicity species at $g \approx 7.0$ ($E/D = 0.05$), which accounts for $96 \pm 10\%$ of the total signal, while the $g = 6$ and $g = 4.3$ signals account for $2 \pm 1\%$ each of the total signal (Figure 3f). The $g \approx 7$ signal for purple N694G at pH 7.2 was identical to the signal at pH 9.2 and therefore had the same species ratio.

Fe(II) Site. The overall crystal structure of N694G (PDB entry 1Y4K) was very similar to the structure of the WT sLO-1 (PDB entry 1F8N); the rms displacement between Cα atoms was 0.41 Å. The largest differences between the structures were found in the loops regions, residues 71−77 and 88−91. The regions of residues 1−6, 21−30, and 117−121 were flexible and invisible in the electron density map, similar to that of the WT sLO-1 structure.

The removal of the Asn side chain at position 694 generated a space that is partially occupied by two water molecules, one of which filled the sixth coordination site of the octahedral Fe(II) cation (Asn694 water, water 1003) (Table 4). The Fe(II)···OH$_2$ distance (2.14 Å) was much
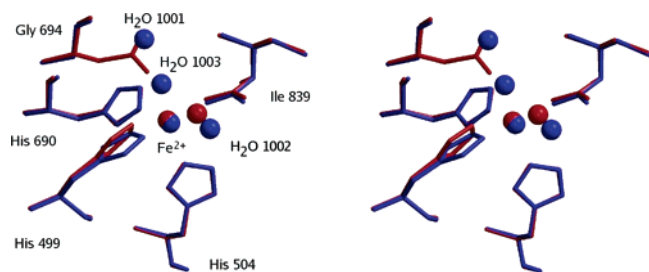
FIGURE 4: Stereoview of WT sLO-1 (1F8N, red) and N694G (1Y4K, blue), superimposed in the area of the active site. For WT sLO-1 (1F8N), a double conformation of His499 is shown. The residues are named according to the N694G structure.
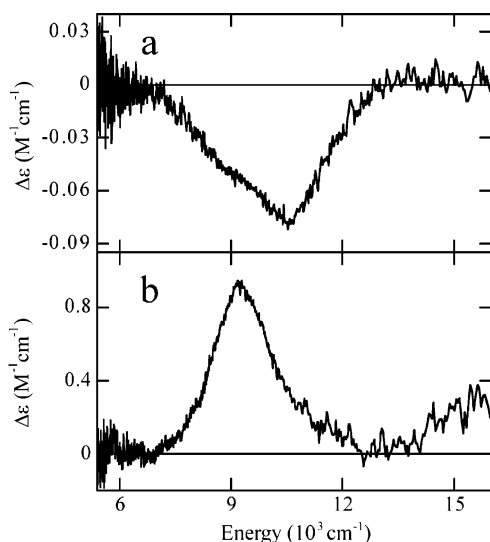

FIGURE 5: (a) Near-infrared CD spectrum of N694G at 278 K and (b) near-infrared MCD spectrum of N694G at 5 K and 7 T.

shorter than the Fe(II)···Oδ1 Asn694 distance (2.87 Å) in the native protein. The second water molecule (water 1001) was hydrogen bonded to the ligated water (1003) and the backbone carbonyl oxygen of Leu754. In comparison with WT sLO-1, there were additional small changes in distances between the Fe(II) ion and other coordinating residues; however, they are minimal (Table 4). The three histidine residues are bound in a facial manner, and the monodentate carboxylate (Ile839) is hydrogen bonded to the active site water (1002). The active centers in N694G and WT sLO-1 are presented for comparison (Figure 4).

Near-infrared CD and MCD spectroscopies were employed to study the high-spin ferrous active site in N694G at higher resolutions and in solution. The CD and MCD results are presented in Figure 5. The energies and splitting pattern of CD/MCD bands provide information about the geometric and electronic structure of the active site in N694G. In octahedral symmetry, a six-coordinate (6C) ferrous site has a doubly degenerate ^5E_g ligand field excited state and a triply degenerate $^5T_{2g}$ ligand field ground state split in energy by 10 Dq ($\sim$10000 cm^{-1}) for biologically relevant nitrogen and oxygen ligands (49, 50). In the low level of symmetry of a protein active site, these states further split ($^5E_g \rightarrow d_{x^2-y^2}$ and d_{z^2}), resulting in two ligand field transitions at $\sim$10000 cm^{-1} and split by $\sim$2000 cm^{-1} for a distorted 6C ferrous site. Five-coordinate (5C) square pyramidal sites show these transitions at $\sim$10000 and $\sim$5000 cm^{-1}, and 5C trigonal bipyramidal sites exhibit one transition at <10000 cm^{-1} and one at <5000

cm^{-1}. Distorted four-coordinate sites exhibit only low-energy ligand field transitions in the 4000–7000 cm^{-1} region, due to the much smaller value of 10 Dq for tetrahedral complexes [10 Dq (T$_d$) = $-^4/_9$ 10 Dq (O$_h$)].

The 278 K CD spectrum of N694G contains two negative ligand field bands at $\sim$8700 and $\sim$10700 cm^{-1} (Figure 5a). CD spectra measured both with and without the glassing agent glycerol present were unchanged. The 5 K, 7 T MCD spectrum of N694G (Figure 5b) contains two positive ligand field features at $\sim$9100 and $\sim$10700 cm^{-1}. Thus, the CD and MCD spectra for N694G reflect the presence of only one species (in contrast to WT sLO), which has a distorted 6C ferrous site with an exogenous water ligand binding to the sixth coordination position previously occupied by Asn694.

DISCUSSION

The coordination environment of the iron binding site in lipoxygenase is highly conserved across plant and mammalian species, with the exception of the sixth ligand (51). The sixth ligand of the active site can vary from an Asn in many plant and mammalian lipoxygenases to a His or a Ser in select mammalian enzymes (19, 21). In sLO-1, the sixth ligand, Asn694, is a weak ligand that can adjust its bond distance to the iron depending on the presence of substrate (linoleic acid) or inhibitor (oleic acid), as observed by MCD (24, 26).

We have proposed that the physical connection between substrate binding and the coordination environment of the iron is a highly conserved hydrogen bonding network that connects the substrate cavity to the first coordination sphere of the iron (Gln495, Gln697, and Asn694) (25). The weak ligation of Asn694 has also been shown to be critical to the activity of sLO-1. Converting the Asn694 ligand to a histidine (N694H) dramatically lowered the enzymatic rate (24, 25). This change in rate was proposed to be due to a decrease in the reduction potential of the active site iron from the stronger His ligation and hence a reduction in the rate of hydrogen abstraction (24).

In this investigation, we studied N694G to further probe the role of the sixth ligand position in the kinetic and spectroscopic properties. With regard to catalysis of LA, the k_{cat} value of N694G is $\sim$230 times lower than that of WT sLO-1 and $\sim$9 times lower than that of N694H at 25 °C (24, 52). The k_{cat}/K_M of N694G is $\sim$45 times lower than that of WT sLO-1 and $\sim$6 times lower than that of N694H at 25 °C (Table 2) (24, 52). These data are indicative of a stronger effect on product release (k_{cat}) than on substrate capture (k_{cat}/K_M) for N694G versus WT sLO-1 and are consistent with the previous trend observed for N694H versus WT sLO-1 (24, 25). In addition, the KIE results for both k_{cat} and k_{cat}/K_M of N694G are consistent with hydrogen atom abstraction being the sole rate-limiting step, indicating that N694G uses the same fundamental mechanism as WT sLO-1 (24).

One of the primary driving forces for the lipoxygenase hydrogen atom abstraction is the reduction potential ($E°$) of the active site iron (53). Previously, we estimated a lower reduction potential for N694H, relative to WT sLO-1, from a shift in the LMCT band (24). This comparison can also be made with regard to N694G (LMCT λ_{max} = 410 nm, 24 390 cm^{-1}), which is higher in energy than WT sLO-1 (LMCT

$\lambda_{\max} = 425$ nm, 23 530 cm^{-1}). This result signifies a lower $E°$ for N694G than for WT sLO-1 and partially contributes to the lowered activity of N694G versus WT sLO-1.

This conclusion is supported by the activation kinetics of N694G. The kinetics of activation of lipoxygenase by 13-(*S*)-HPOD measures both the K_D of 13-(*S*)-HPOD binding and the rate at which 13-(*S*)-HPOD oxidizes the ferrous active site iron (k_2). The activation data of N694G demonstrate that the active site of N694G is comparable to that of WT sLO-1 with the K_D values being similar for both ($K_D = 41 \pm 5$ μM for N694G and $K_D = 39 \pm 14$ μM for WT sLO-1). Nevertheless, the rate of iron oxidation for N694G is faster than that of WT sLO-1 ($k_2 = 606 \pm 18$ s^{-1} for N694G and $k_2 = 349 \pm 31$ s^{-1} for WT sLO-1). These kinetic results, coupled with the blue-shifted His-to-Fe(III) LMCT band, indicate a lowered reduction potential for N694G and suggest a stronger ligand at the active site iron than the native Asn694.

This hypothesis is confirmed by the crystal structure, the CD/MCD data for ferrous N694G, and the EPR signal of ferric N694G. The ferrous structure shows two water molecules in the cavity, occupied by Asn694 in WT sLO-1, with one of the waters bound directly to the iron. The water ligated to the ferrous iron has a short bond distance relative to the Asn in WT sLO-1 (Table 4), indicating a strong ligand interaction and hence a lowered reduction potential (i.e., lowered kinetic activity). Furthermore, the crystallographically defined iron coordination correlates well with CD and MCD studies of N694G, which are consistent with the presence of a purely 6C ferrous site with an exogenous water ligand bound in solution.

The solution EPR spectrum of ferric N694G at pH 9.2 shows a distribution of species with the intermediate rhombic signal being the major component (64%). The intermediate rhombicity species has an E/D value of 0.05, which is similar to the intermediate rhombic signal of N694H ($E/D = 0.08$) (*24*) but is in contrast to the axial signal ($E/D = 0.01$) of the WT sLO-1 enzyme (*54*). The axial signal in the wild type reflects the presence of an open coordination position on Fe-(III) (i.e., 5C square pyramidal). These data indicate that the coordination environment of N694G is 6C (not axial) but with one strong unique axis (not completely rhombic), as seen previously with N694H (*24*). Considering the fact that the yellow N694G EPR is minimally pH dependent and yellow WT sLO-1 has a hydroxide bound, it is appropriate to assume that the 6C coordination environment of ferric N694G contains one hydroxide and one water with the hydroxide corresponding to the strong axis; however, it is unclear which coordination position (active site or Asn694) has the water and which has the hydroxide.

The purple species of N694G manifests the same three species as the yellow form: axial ($E/D = 0$), intermediate rhombicity ($E/D = 0.05$), and rhombic ($E/D = 0.33$); however, its appearance is different from the yellow signal due to the increase in the percentage of the intermediate rhombicity species (96%) and the lowered *g* strain (Table 3), which sharpens certain features of the signal. If we assume 13-(*S*)-HPOD is directly bound to the iron, on the basis of the purple LMCT band, then 13-(*S*)-HPOD has displaced the exogenous, water-derived, ligand, similar to that seen in the 13-(*S*)-HPOD−WT sLO-3 structure (*55*). The fact that the E/D of the intermediate rhombicity species
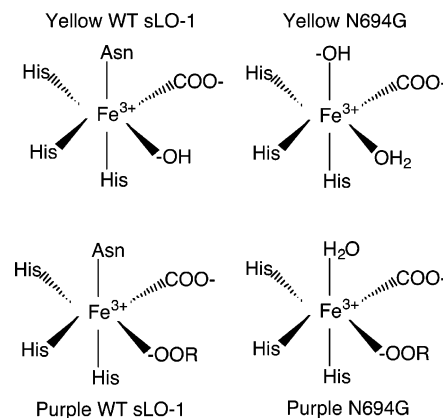

FIGURE 6: Proposed coordination geometry of the Fe(III) center for WT sLO-1 and N694G.

does not change with anionic, hydroperoxide binding suggests that a hydroxide has been lost in the coordination environment, leaving 13-(*S*)-HPOD bound to the catalytic site position and a water at position 694 (Figure 6). This is supported by the fact that the purple N694G EPR does not change down to pH 7.2, indicating a bound water. Nevertheless, the fact that the exogenous, Asn694 ligand is a water in purple N694G does not indicate that the exogenous, Asn694 ligand is a water in the yellow form because the decrease in the Lewis acidity of the ferric iron upon 13-(*S*)-HPOD binding could increase the pK_a of a hydroxide, leading to its protonation.

This raises the question of which ligation position, the catalytic site or position 694, is the hydroxide and which is the water in the ferric, yellow form of N694G. A possible answer to this question may be found in analysis of the kinetics of N694G. The activation parameters are twice as fast for N694G as for WT sLO-1, while the catalysis of LA hydroperoxidation is more than 230 times slower. These results, combined with the higher rhombicity of the ferric, yellow, N694G EPR signal and a blue shift in the LMCT band, compared to those of WT sLO-1, support our previous hypothesis that stronger ligands (than Asn) at position 694 in sLO-1 lower the reduction potential and thus decrease the driving force of the reaction (*24*). Nevertheless, N694G is more than 9-fold slower than N694H even though its LMCT band is lower in energy (410 and 400 nm, respectively). If the reduction potential were the only factor in the rate of catalysis, one would hypothesize that the rate of catalysis of N694G would be faster than that of N694H, which is not the case. This suggests that there is another factor that affects the rate of catalysis of N694G. One possibility is that in the ferric state, the water is the active site-oriented ligand and the hydroxide is the Asn694 ligand. We and others have proposed that the active site hydroxide is critical to abstraction of the hydrogen atom from the substrate (*9, 25*). If this critical, active site, exogenous ligand is in fact a water in N694G, then the rate of hydrogen atom abstraction would be lowered dramatically. This hypothesis is supported by examination of the hydrogen bond interactions with both water ligands in the ferrous forms of N694G (Figure 7). The active site water is hydrogen bonded to the bound carboxylate (Ile839), which would increase its pK_a due to anionic repulsion, favoring protonation. This same H-bond is shorter for N694G (2.25 Å) than for WT sLO (2.50 Å), which would
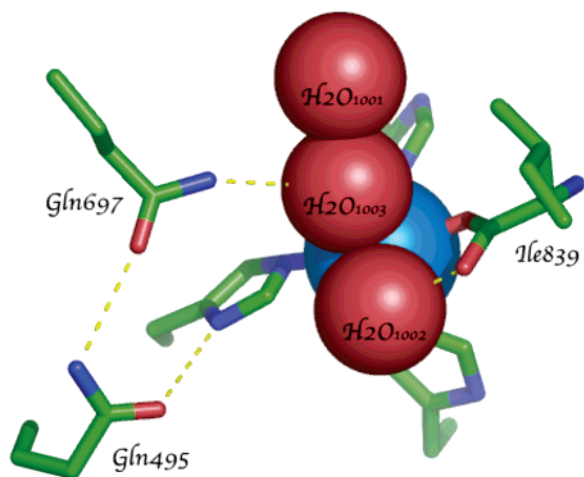
FIGURE 7: Coordination geometry of the Fe(II) center of N694G. Bonds between the iron and first-sphere ligands are depicted as solid lines, and hydrogen bonding interactions are depicted as dashed lines among water1003, Gln697, Gln495, and His499. Oxygen atoms are colored red, nitrogens blue, and carbons green, and the iron atom is colored cyan.

increase the pK_a of the active site water in N694G even more (Figure 4). In contrast, the Asn694 water, for N694G, is hydrogen bonded to a second water and has a distant hydrogen bond from the NH group of Gln697, which could potentially stabilize the charge of a bound hydroxide, upon oxidation of the iron. On the basis of these structural factors, the Asn694 water ligand would likely become the bound hydroxide in the ferric state (Figure 6), hence accounting for the lowered reaction rate of N694G compared to that of N694H, even though its reduction potential is not as low. We are currently investigating this possibility.

ACKNOWLEDGMENT

SUPPORTING INFORMATION AVAILABLE

A graph of the temperature dependence of the KIE data is available free of charge via the Internet at http://pubs.acs.org.

REFERENCES

1. Grechkin, A. (1998) Recent developments in biochemistry of the plant lipoxygenase pathway, *Prog. Lipid Res. 37*, 317−352.
2. Kessler, A., Halitschke, R., and Baldwin, I. T. (2004) Silencing the jasmonate cascade: Induced plant defenses and insect population, *Science 305*, 665−668.
3. Wenzel, S. E. (2003) The role of leukotrienes in asthma, *Prostaglandins, Leukotrienes Essent. Fatty Acids 69*, 145−155.
4. Kuhn, H. (2004) Lipoxygenases in the cardiovascular system, *Circ. Res. 94*, 1527−1529.
5. Tang, D. G., La, E., Kern, J., and Kehrer, J. (2002) Fatty acid oxidation and signaling in apoptosis, *Biol. Chem. 383*, 425−442.
6. Solomon, E. I., Decker, A., and Lehnert, N. (2003) Non-heme iron enzymes: Contrasts to heme catalysis, *Proc. Natl. Acad. Sci. U.S.A. 100*, 3589−3594.
7. DeGroot, J. J., Veldink, G. A., Vliegenhart, J. F. G., Boldingh, J., Wever, R., and Van Gelder, B. F. (1975) Demonstration by EPR spectroscopy of functional role of iron in soybean lipoxygenase-1, *Biochim. Biophys. Acta 377*, 71−79.
8. Ruddat, V. C., Whitman, S., Holman, T. R., and Bernasconi, C. F. (2003) Stopped-flow kinetic investigations of the activation of soybean lipoxygenase-1 and the influence of inhibitors on the allosteric site, *Biochemistry 42*, 4172−4178.
9. Scarrow, R. C., Trimitsis, M. G., Buck, C. P., Grove, G. N., Cowling, R. A., and Nelson, M. J. (1994) X-ray Spectroscopy of the Iron Site in Soybean Lipoxygenase-1: Changes in Coordination Upon Oxidation or Addition of Methanol, *Biochemistry 33*, 15023−15035.
10. Glickman, M. H., and Klinman, J. P. (1996) Lipoxygenase reaction mechanism: Demonstration that hydrogen abstraction from substrate precedes dioxygen binding during catalytic turnover, *Biochemistry 35*, 12882−12892.
11. Rickert, K. W., and Klinman, J. P. (1999) Nature of hydrogen transfer in soybean lipoxygenase-1: Separation of primary and secondary isotope effects, *Biochemistry 38*, 12218−12228.
12. Lewis, E. R., Johansen, E., and Holman, T. R. (1999) Large competitive kinetic isotope effects in human 15-LO catalysis measured by a novel HPLC method, *J. Am. Chem. Soc. 121*, 1395−1396.
13. Segraves, E. N., and Holman, T. R. (2003) Kinetic investigations of the rate-limiting step in human 12- and 15-lipoxygenase, *Biochemistry 42*, 5236−5243.
14. Knapp, M. J., Seebeck, F. P., and Klinman, J. P. (2001) Steric control of oxygenation regiochemistry in soybean lipoxygenase-1, *J. Am. Chem. Soc. 123*, 2931−2932.
15. Knapp, M. J., and Klinman, J. P. (2003) Kinetic studies of oxygen reactivity in soybean lipoxygenase-1, *Biochemistry 42*, 11466−11475.
16. Minor, W., Steczko, J., Boguslaw, S., Otwinowski, Z., Bolin, J. T., Walter, R., and Axelrod, B. (1996) Crystal structure of soybean lipoxygenase L-1 at 1.4 Å resolution, *Biochemistry 35*, 10687−10701.
17. Skrzypczak-Jankun, E., Amzel, L. M., Kroa, B. A., and Funk, M. O. (1997) Structure of Soybean Lipoxygenase L3 and a Comparison with Its L1 Isoenzyme, *Proteins 29*, 15−31.
18. Gillmor, S. A., Villasenor, A., Fletterick, R., Sigal, E., and Browner, M. (1997) The structure of mammalian 15-lipoxygenase reveals similarity to the lipases and the determinants of substrate specificity, *Nat. Struct. Biol. 4*, 1003−1009.
19. Sloane, D. L. (1996) Exploring the structure and function of mammalian lipoxygenases by site-directed mutagenesis, in *Lipoxygenases and Lipoxygenase Pathway Enzymes* (Piazza, G., Ed.) pp 57−79, AOCS Press, Champaign, IL.
20. Brash, A. R., Boeglin, W. E., and Chang, M. S. (1997) Discovery of a Second 15s-Lipoxygenase in Humans, *Proc. Natl. Acad. Sci. U.S.A. 94*, 6148−6152.
21. Tang, S. H., Bhatia, B., Maldonaldo, C. J., Yang, P. Y., Newman, R. A., Liu, J. W., Chandra, D., Traag, J., Klein, R. D., Fischer, S. M., Chopra, D., Shen, J. J., Zhau, H. E., Chung, L. W. K., and Tang, D. G. (2002) Evidence that arachidonate 15-lipoxygenase 2 is a negative cell cycle regulator in normal prostate epithelial cells, *J. Biol. Chem. 277*, 16189−16201.
22. Jisaka, M., Boeglin, W. E., Kim, R. B., and Brash, A. R. (2001) Site-directed mutagenesis studies on a putative fifth iron ligand of mouse 8S-lipoxygenase: Retention of catalytic activity on mutation of serine-558 to asparagine, histidine, or alanine, *Arch. Biochem. Biophys. 386*, 136−142.
23. Pavlosky, M. A., Zhang, Y., Westre, T. E., Gan, Q.-F., Pavel, E. G., Campochiaro, C., Hedman, B., Hodgson, K. O., and Solomon, E. I. (1995) Near-IR CD, MCD and X-ray absorption spectral comparison of the non-heme ferrous active sites of plant and mammalian 15-lipoxygenases, *J. Am. Chem. Soc. 117*, 4316−4327.
24. Holman, T. R., Zhou, J., and Solomon, E. I. (1998) Spectroscopic and functional characterization of a ligand coordination mutant of soybean lipoxygenase: First coordination sphere analogue of human 15-lipoxygenase, *J. Am. Chem. Soc. 120*, 12564−12572.
25. Tomchick, D. R., Phan, P., Cymborowski, M., Minor, W., and Holman, T. R. (2001) Structural and functional characterization of second coordination sphere mutants of soybean lipoxygenase-1, *Biochemistry 40*, 7509−7517.
26. Schenk, G., Neidig, M. L., Zhou, J., Holman, T. R., and Solomon, E. I. (2003) Spectroscopic characterization of soybean lipoxygenase-1 mutants: The role of second coodination sphere residues in the regulation of enzyme activity, *Biochemistry 42*, 7294−7302.
27. Zhang, Y., Gan, Q. F., Pavel, E. G., Sigal, E., and Solomon, E. I. (1995) EPR definition of the non-heme ferric active sites of mammalian 15-lipoxygenase: Major spectral difference relative to human 5-lipoxygenases and plant lipoxygenases and their ligand field origin, *J. Am. Chem. Soc. 117*, 7422−7427.
28. Ruddat, V. C., Mogul, R., Chorny, I., Chen, C., Perrin, N., Whitman, S., Kenyon, V., Jacobson, M. P., Bernasconi, C. F.,

and Holman, T. R. (2004) Tryptophan 500 and arginine 707 define product and substrate active site binding in soybean lipoxygenase-1, *Biochemistry 43*, 13063−13071.

29. Mogul, R., and Holman, T. R. (2001) Inhibition studies of soybean and human 15-lipoxygenase with long-chain alkenyl sulfate substrates, *Biochemistry 40*, 4391−4397.

30. Glickman, M. H., and Klinman, J. P. (1995) Nature of rate-limiting steps in the soybean lipoxygenase-1 reaction, *Biochemistry 34*, 14077−14092.

31. Otwinowski, Z., and Minor, W. (1997) *Processing of X-ray diffraction data collected in oscillation mode*, Vol. 276, Macromolecular Crystallography, Part A, Academic Press, New York.

32. Murshudov, G. N., Vagin, A. A., and Dodson, E. J. (1997) Refinement of macromolecular structures by the maximum-likelihood method, *Acta Crystallogr. D53*, 240−255.

33. Jones, T. A., Zou, J. Y., Cowan, S. W., and Kjeldgaard, M. (1991) Improved methods for building protein models in electron density maps and the location of errors in these models, *Acta Crystallogr. A47*, 110−119.

34. Emsley, P., and Cowtan, K. (2004) Coot: Model-building tools for molecular graphics, *Acta Crystallogr. D60*, 2126−2132.

35. Brünger, A. T. (1992) Free R value: A novel statistical quantity for assesing the accuracy of crystal structures, *Nature 335*, 472−475.

36. Laskowski, R. A., MacArthur, M. W., Moss, D. S., and Thornton, J. M. (1993) PROCHECK: A program to check the stereochemical quality of protein structures, *J. Appl. Crystallogr. 26*, 283−291.

37. Lovell, S. C., Davis, I. W., Arendall, W. B., III, de Bakker, P. I., Word, J. M., Prisant, M. G., Richardson, J. S., and Richardson, D. C. (2003) Structure validation by Ca geometry: ϕ,ψ and Cb deviation, *Proteins 50*, 437−450.

38. Kabsch, W. (1976) A solution for the best rotation to relate two sets of vectors, *Acta Crystallogr. A32*, 922−923.

39. Collaborative Computational Project, Number 4 (1994) The CCP4 suite: Programs for protein cystallography, *Acta Crystallogr. D50*, 760−763.

40. DeLano, W. L. (2002) *PyMol*, DeLano Scientific, San Carlos, CA.

41. Egmond, M. E., Fasella, P. M., Veldink, G. A., Vliegenhart, J. F. G., and Boldingh, J. (1977) On the Mechanism of Action of Soybean Lipoxygenase-1, *Eur. J. Biochem. 76*, 469−479.

42. Verhagen, J., Vliegenthart, J. F. G., and Boldingh, J. (1978) Micelle and acid-soap formation of linoleic acid and 13-ʟ-hydro-peroxy-linoleic acid being substrates of lipoxygenase-1, *Chem. Phys. Lipids 22*, 255−259.

43. Kohen, A., and Klinman, J. P. (1999) Hydrogen tunneling in biology, *Chem. Biol. 6*, R191−R198.

44. Jonsson, T., Glickman, M. H., Sun, S. J., and Klinman, J. P. (1996) Experimental evidence for extensive tunneling of hydrogen in the lipoxygenase reaction: Implications for enzyme catalysis, *J. Am. Chem. Soc. 118*, 10319−10320.

45. Gardner, H. W. (1989) Soybean Lipoxygenase-1 Enzymatically Forms Both (9S)- and (13S)-Hydroperoxides From Linoleic Acid by a pH-Dependent Mechanism, *Biochim. Biophys. Acta 1001*, 274−281.

46. Wang, Z. X., Killilea, S. D., and Srivastava, D. K. (1993) Kinetic Evaluation of Substrate-Dependent Origin of the Lag Phase in Soybean Lipoxygenase-1 Catalyzed Reations, *Biochemistry 32*, 1500−1509.

47. Aasa, R., and Vanngard, T. (1975) EPR signal intensity and powder shapes: A reexamination, *J. Magn. Reson. 19*, 308−315.

48. Slappendel, S., Veldink, G. A., Vliegenhardt, J. F. G., Aasa, R., and Malmström, B. G. (1980) EPR spectroscopy of soybean lipoxygenase-1, *Biochim. Biophys. Acta 642*, 30−39.

49. Pavel, E. G., Kitajima, N., and Solomon, E. I. (1998) Magnetic circular dichroism spectroscopic studies of mononuclear non-heme ferrous model complexes. Correlation of excited- and ground-state electronic structure with geometry, *J. Am. Chem. Soc. 120*, 3949−3962.

50. Solomon, E. I., Pavel, E. G., Loeb, K. E., and Campochiaro, C. (1995) Magnetic Circular Dichroism Spectroscopy as a Probe of the Geometric and Electronic Structure of Non-Heme Ferrous Enzymes, *Coord. Chem. Rev. 144*, 369−460.

51. Steczko, J., Donoho, G. P., Clemens, J. C., Dixon, J. E., and Axelrod, B. (1992) Conserved histidine residues in soybean lipoxygenase: Functional consequences of their replacement, *Biochemistry 31*, 4053−4057.

52. Knapp, M. J., Rickert, K., and Klinman, J. P. (2002) Temperature-dependent isotope effects in soybean lipoxygenase-1: Correlating hydrogen tunneling with protein dynamics, *J. Am. Chem. Soc. 124*, 3865−3874.

53. Gardner, K. A., and Mayer, J. M. (1995) Understanding C−H bond oxidations: Hydrogen and hydride transfer in the oxidation of toluene by permanganate, *Science 269*, 1849−1851.

54. Gaffney, B. J., and Silverstone, H. J. (1993) Simulation of the EMR spectra of high-apin iron in proteins, in *EMR of Paramagnetic Molecules* (Berliner, L. J., and Reuben, J., Eds.) pp 1−57, Springer, Berlin.

55. Skrzypczak-Jankun, E., Bross, R. A., Carroll, R. T., Dunham, W. R., and Funk, M. O., Jr. (2001) Three-dimensional structure of a purple lipoxygenase, *J. Am. Chem. Soc. 123*, 10814−10820.

BI060577E